nature neuroscience

Oligodendrocyte progenitors balance growth with self-repulsion to achieve homeostasis in the adult brain

Ethan G Hughes[1,3], Shin H Kang[1–3], Masahiro Fukaya[1–3] & Dwight E Bergles[1]

The adult CNS contains an abundant population of oligodendrocyte precursor cells (NG2$^+$ cells) that generate oligodendrocytes and repair myelin, but how these ubiquitous progenitors maintain their density is unknown. We generated *NG2-mEGFP* mice and used *in vivo* two-photon imaging to study their dynamics in the adult brain. Time-lapse imaging revealed that NG2$^+$ cells in the cortex were highly dynamic; they surveyed their local environment with motile filopodia, extended growth cones and continuously migrated. They maintained unique territories though self-avoidance, and NG2$^+$ cell loss though death, differentiation or ablation triggered rapid migration and proliferation of adjacent cells to restore their density. NG2$^+$ cells recruited to sites of focal CNS injury were similarly replaced by a proliferative burst surrounding the injury site. Thus, homeostatic control of NG2$^+$ cell density through a balance of active growth and self-repulsion ensures that these progenitors are available to replace oligodendrocytes and participate in tissue repair.

Homeostatic control of cell density is an essential feature of tissue and organ maintenance, allowing cell replacement and regeneration to offset cell loss resulting from injury, disease or age-dependent degeneration[1,2]. Tight control over cell proliferation is especially critical in the adult CNS, which has a limited capacity to accommodate growth as a result of its complex cellular architecture and its encasement in bone. In contrast with neurons, which, apart from restricted populations in the hippocampus and olfactory bulb, are not replaced even in the context of injury and disease[3], many glial cells exhibit a remarkable capacity for self-renewal[4,5]. However, it is not known how the density and distribution of different classes of glial cells are maintained in the adult CNS.

Glial progenitor cells that express the chondroitin sulfate proteoglycan NG2, termed NG2$^+$ cells (or oligodendrocyte precursor cells), comprise the majority of proliferating cells in the adult CNS[6]. During development, these glial cells migrate from germinal zones, proliferate and differentiate into myelinating oligodendrocytes[7–9]. Although myelinated tracts are formed early in life, NG2$^+$ cells are retained throughout the adult CNS, where they are organized in a grid-like or tiled manner, with individual cells occupying non-overlapping domains[10]. *In vivo* genetic fate tracing studies indicate that NG2$^+$ cells continue to differentiate into oligodendrocytes in adults[7,11–13] and are rapidly mobilized to replace oligodendrocytes in animal models of acute and chronic demyelination[4,14,15], suggesting that they are important for both normal oligodendrocyte homeostasis and the regeneration of myelin. Although continual renewal of these progenitors is likely to be crucial for efficient oligodendrogenesis, the mechanisms that control their uniform distribution and high density in the adult CNS remain unknown, in part because their dynamics have not been examined in the intact adult CNS[9,16,17].

NG2$^+$ cell proliferation is enhanced following demyelination[15], traumatic injury to the CNS[18] and in chronic neurodegenerative disease[7,19]; however, the relationship between proliferation of these progenitors and the generation of new oligodendrocytes remains uncertain[20]. Moreover, uncontrolled growth of these progenitors leads to tumor formation[21], and recent studies have suggested that NG2$^+$ cells are likely to be a cell of origin for certain forms of glioma[22,23], highlighting the importance of understanding how the proliferation of these cells is controlled *in vivo*.

To address these questions, we developed a line of transgenic mice that express a membrane-anchored form of EGFP under the control of the NG2 (*Cspg4*) promoter (*NG2-mEGFP-H* mice) and performed *in vivo* two-photon imaging of NG2$^+$ cells in the mouse somatosensory cortex. We found that NG2$^+$ cells were highly dynamic in the adult brain; they extended motile filopodia, reorganized their processes and continuously moved through the parenchyma. Although their position was not fixed, NG2$^+$ cells maintained independent domains through self-repulsion, and loss of cells through death, differentiation or experimental ablation triggered rapid migration and proliferation of adjacent NG2$^+$ cells to preserve their density. Long-term imaging revealed that NG2$^+$ cells directly differentiated into oligodendrocytes without proliferation, indicating that division of these progenitors is a homeostatic response to cell removal, rather than the generation of oligodendrocytes through asymmetric division. Although adult NG2$^+$ cells can serve as oligodendrocyte progenitors, they also migrated to sites of focal injury to help form a glial scar and were similarly replaced through proliferation of neighboring NG2$^+$ cells. By balancing active growth with self-repulsion, NG2$^+$ cells maintain a constant density in the CNS, ensuring that they are available to participate in regeneration and repair of the CNS throughout life.

[1]The Solomon H. Snyder Department of Neuroscience, Johns Hopkins University School of Medicine, Baltimore, Maryland, USA. [2]Present addresses: Center for Neural Repair and Rehabilitation, Temple University School of Medicine, Philadelphia, Pennsylvania, USA (S.H.K.) and Department of Anatomy, Kitasato University School of Medicine, Sagamihara, Japan (M.F.). [3]These authors contributed equally to this work. Correspondence should be addressed to D.E.B. (dbergles@jhmi.edu).

Received 16 January; accepted 28 March; published online 28 April 2013; corrected online 6 May 2013; doi:10.1038/nn.3390

RESULTS

Adult NG2$^+$ cells extend processes with dynamic filopodia

To define the behavior of NG2$^+$ cells in the adult brain, we generated BAC transgenic mice that express a membrane-anchored form of EGFP[24] under the control of the NG2 promoter (*NG2-mEGFP-H* mice; **Supplementary Fig. 1**), which allowed visualization of the full extent of their complex morphologies (**Supplementary Fig. 2**). *In vivo* two-photon imaging through a cranial window revealed that fluorescent NG2$^+$ cells were distributed in a highly ordered manner throughout the upper layers of the cortex of these mice (**Supplementary Movie 1**), with cells occupying non-overlapping domains. NG2$^+$ cells extended highly ramified processes studded with numerous filopodia-like protrusions into the surrounding neuropil (**Fig. 1a**). In time-lapse recordings, these thin protrusions were highly dynamic, continually extending, retracting, branching and altering their trajectory (**Fig. 1a–c** and **Supplementary Movies 2** and **3**) with an average speed of 0.3 ± 0.01 µm min^{-1} (185 protrusions on 10 cells in 5 mice). Motile filopodia were present along the length of each process and even extended from the soma (**Fig. 1a**,**d**,**e**), indicating that NG2$^+$ cells actively survey their local environment. This dynamic behavior is similar to that exhibited by microglial cells[25,26], although NG2$^+$ cell filopodia lacked the bulbous endings that are characteristic of microglial processes and moved more slowly (microglia process speed = 1.47 ± 0.1 µm min^{-1}; from ref. 26).

Despite the active growth of NG2$^+$ cell processes, these cells maintained a radial morphology and contacts between processes were rarely observed. Previous studies found that contact-mediated inhibition can help establish a radial morphology and control cell spacing through homotypic repulsion[27,28]. In time-lapse imaging, growing filopodia of NG2$^+$ cells always retracted when they contacted a process of the same or an adjacent NG2$^+$ cell (**Fig. 1f**,**g** and **Supplementary Movie 3**), indicating that these progenitors engage in continual self-avoidance through contact-mediated inhibition.

Previous studies have shown that removal of the skull and implantation of a chronic cranial window can induce reactive changes in glial cells and enhance the dynamics of dendritic spines on neurons[29]. To determine whether the dynamic behavior of NG2$^+$ cells was a reactive response to injury, we prepared *NG2-mEGFP-H* mice with thinned-skull cranial windows[30] and performed time-lapse imaging. NG2$^+$ cells imaged through the skull had complex morphologies and highly dynamic filopodia were observed along their processes, both of which were comparable to those observed in mice implanted with chronic cranial windows (**Supplementary Fig. 3** and **Supplementary Movie 4**). Moreover, mice implanted with chronic cranial windows did not show reactive changes in microglia or increases in the number of proliferating cells relative to controls when *in vivo* imaging was initiated (**Supplementary Fig. 4**). These results indicate that

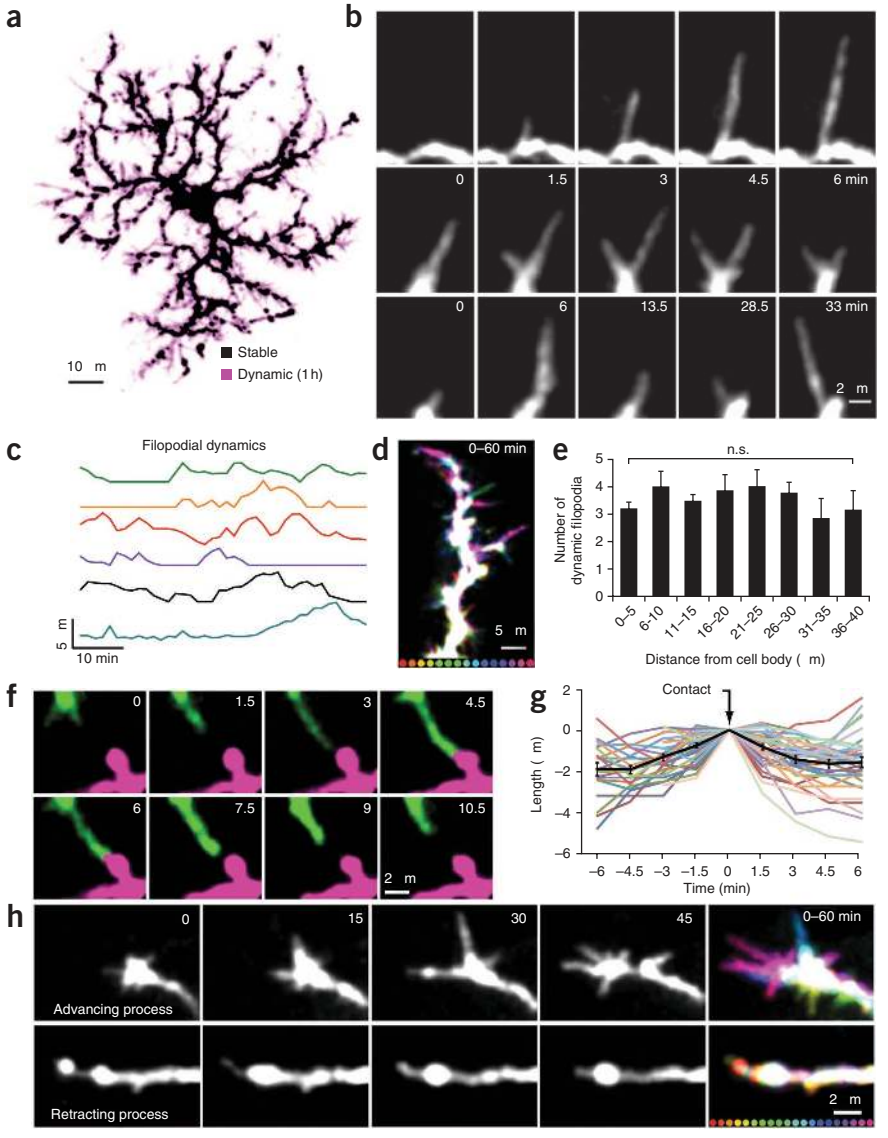

Figure 1 NG2$^+$ cells extend dynamic filopodia and exhibit self-repulsion in the adult cortex. (**a**) Maximum-intensity projection of an individual NG2$^+$ cell during 1 h of time-lapse imaging. Stable regions are shown in black and dynamic regions are shown in magenta. (**b**) Individual NG2$^+$ cell filopodia extended (top), branched (middle) and altered their trajectory (bottom) in minutes. (**c**) Plots showing the change in length over time of six NG2$^+$ cell filopodia. (**d**) Maximum-intensity projection of one NG2$^+$ cell process, color coded for time (intervals below = 4 min). Stable areas are represented in white. (**e**) Graph showing the distribution of dynamic filopodia along NG2$^+$ cell processes ($n = 13$ branches on 7 cells in 5 mice, n.s. indicates not significant ($P > 0.05$), one-way ANOVA with Tukey *post hoc* test). Error bars represent s.e.m. (**f**) *In vivo* time-lapse images of two pseudo-colored NG2$^+$ cell processes. Contact led to filopodial retraction. (**g**) Plot of the change in length of NG2$^+$ cell filopodia before and after contacting another NG2$^+$ cell processes ($n = 35$ filopodia on 10 cells in 5 mice). Average change in length for all processes is shown in black. (**h**) *In vivo* time-lapse imaging of advancing (top) and retracting (bottom) NG2$^+$ cell processes. Montages at far right (0–60 min) are maximum-intensity projection images showing two NG2$^+$ cell processes color coded for time (intervals below = 3 min). Stable areas are represented in white. Note the presence of highly motile filopodia at the tip of the advancing process and the absence of filopodia on the retracting process.

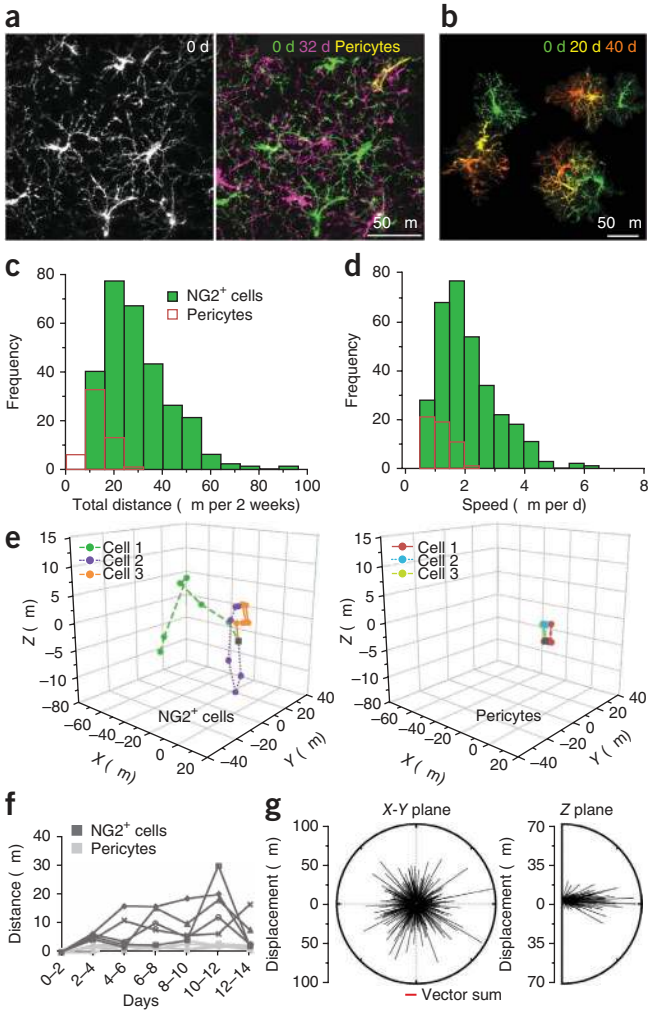

Figure 2 NG2+ cells continually change their position in the adult cortex. (**a**) Image of NG2+ cells in one region of cortex on day 0 (left) and 32 d later (right, montage of two time points). Stable pericytes are shown in yellow. (**b**) Montage showing the change in morphology and position of three NG2+ cells over 40 d. (**c**) Histogram showing the distances that NG2+ cells (green bars) and perivascular cells (red bars) moved over 2 weeks (318 NG2+ cells, 53 perivascular cells in 5 mice, $P < 0.05$, Mann-Whitney test). (**d**) Histogram of the speed that NG2+ cells and pericytes moved over 2 weeks (318 NG2+ cells, 53 perivascular cells in 5 mice, $P < 0.05$, Mann-Whitney test). (**e**) Three-dimensional graphs showing the movements of three NG2+ cells (left) and three perivascular cells (right) in the somatosensory cortex over a 2-week period. (**f**) Graph showing the displacement of somata over time for five NG2+ cells and five pericytes. (**g**) Vector plots of the direction and displacement of 905 NG2+ cell movements in the *X-Y* plane (left, $P = 0.578$, Moore-Rayleigh test) and the *Z* plane (right) for cells >90 µm below the pia mater.

the extension of dynamic filopodia from NG2+ cell processes is a normal feature of these progenitors in the uninjured brain, rather than a reactive response to cranial window implantation.

NG2+ cells migrate continuously through the adult cortex

The tips of advancing NG2+ cell processes displayed numerous motile filopodia, reminiscent of neuronal growth cones, whereas retracting processes lacked filopodia (**Fig. 1h**), suggesting that these dynamics may enable cell migration. To determine whether process motility is accompanied by somatic translocation, we re-imaged NG2+ cells in the same volume of tissue 1 month later. Although the position of vascular-associated pericytes in these regions was unchanged, the distribution of NG2+ cell somata and the orientation of their processes were markedly altered, and it was not possible to unambiguously identify the same NG2+ cells from the previous imaging session (**Fig. 2a**).

More frequent imaging revealed that NG2+ cells continually reoriented their processes and moved an average distance of 2.1 ± 0.1 µm d^{-1} (318 NG2+ cells in 5 mice; **Fig. 2b–d** and **Supplementary Movies 5** and **6**), in contrast with pericytes, which remained largely stationary (**Fig. 2e,f**). Individual NG2+ cells exhibited heterogeneous behaviors, with some cells moving at a continuous rate during the 2-week imaging period, whereas others interrupted periods of relative stability with large movements of >30 µm over a period of a few days (**Fig. 2f**). Long-range cues guide the migration of NG2+ cells during development[31], raising the possibility that similar gradients influence their movement in the adult CNS. However, analysis of the trajectories of all NG2+ cells in a 0.06-mm^3 cortical volume revealed that there was no directional bias in their movement (**Fig. 2g**), suggesting that their behavior is controlled by local interactions rather than large-scale gradients of attractive or repulsive cues.

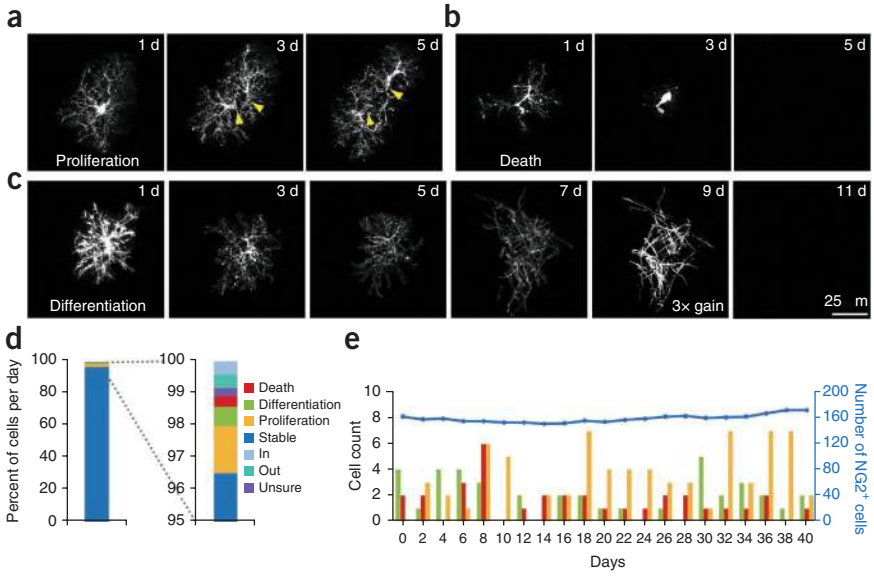

Figure 3 NG2+ cell density is maintained despite proliferation, differentiation, and death. (**a**–**c**) Sequential images from *in vivo* time-lapse recordings illustrating individual NG2+ cells undergoing division (**a**), death (**b**) and differentiation (**c**). The image intensity at 9 d in **c** was increased threefold to illustrate the transition to an oligodendrocyte morphology. EGFP intensity decreased with differentiation as a result of downregulation of the *NG2* promoter[10]. (**d**) Graph illustrating the proportion of NG2+ cells engaged in different behaviors on each day (1,118 NG2+ cells in 5 mice). (**e**) Combined plot showing the number of NG2+ cells undergoing proliferation, differentiation and death (colored bars) and the total NG2+ cell density (blue line) in a 0.06-mm^3 volume of adult somatosensory cortex over a 40-d period.

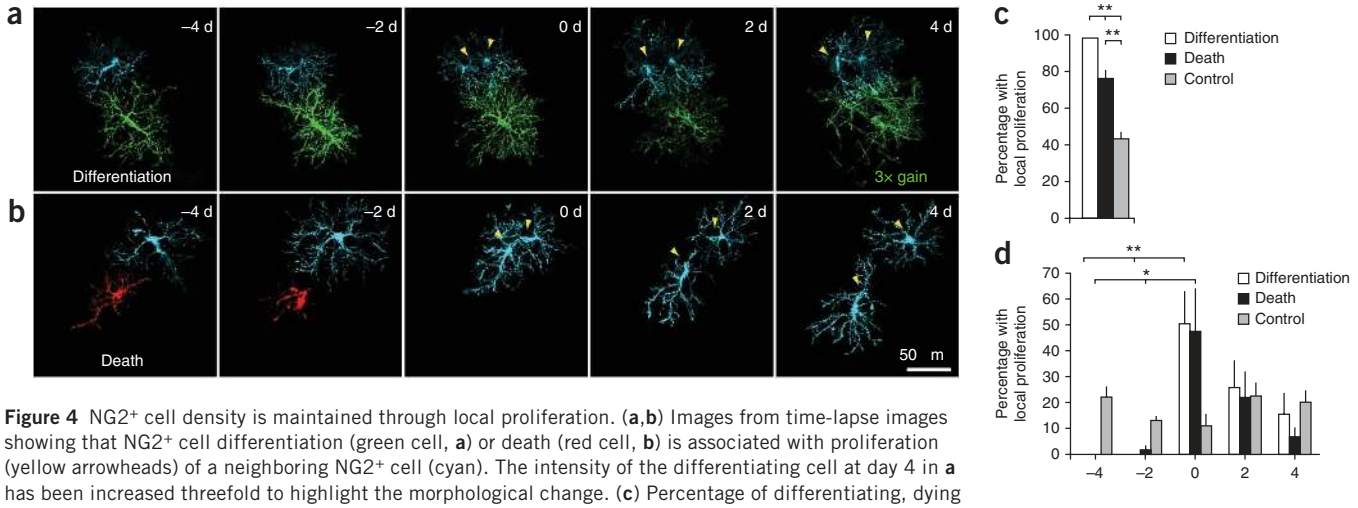

Figure 4 NG2⁺ cell density is maintained through local proliferation. (**a**,**b**) Images from time-lapse images showing that NG2⁺ cell differentiation (green cell, **a**) or death (red cell, **b**) is associated with proliferation (yellow arrowheads) of a neighboring NG2⁺ cell (cyan). The intensity of the differentiating cell at day 4 in **a** has been increased threefold to highlight the morphological change. (**c**) Percentage of differentiating, dying and stable NG2⁺ cells that were associated with proliferation of a neighboring NG2⁺ cell (72 differentiating, 54 dying, 187 stable NG2⁺ cells in 5 mice; $^{**}P < 0.005$ one-way ANOVA with Tukey *post hoc* test). (**d**) Time course of local proliferation relative to the onset of cell loss through death or differentiation ($^{*}P < 0.03$, $^{**}P < 0.005$, one-way ANOVA with Tukey *post hoc* test). Error bars represent s.e.m.

Constant turnover of NG2⁺ cells in the adult brain

In addition to the constant reorganization of NG2⁺ cell position in the cortex, there were dynamic changes in the overall population resulting from the proliferation, differentiation and death of individual NG2⁺ cells (**Fig. 3a–c**). Cell death was characterized by hypertrophy, retraction of processes and abrupt disappearance of the cell (**Supplementary Fig. 5**), whereas differentiation into oligodendrocytes was accompanied by a gradual decrease in fluorescence, transformation of their highly ramified processes to long, unbranched processes and expression of myelin proteins (**Supplementary Fig. 6**). NG2⁺ cells did not differentiate into astrocytes or neurons in this region, providing further evidence that these glial cells serve as lineage-restricted progenitors in the normal CNS[7]; however, if EGFP is degraded more rapidly during transdifferentiation, adoption of these alternate fates would be difficult to assess using this approach.

In contrast with the segregation of principal neurons into distinct cortical lamina, NG2⁺ cells were evenly distributed among cortical layers, and the core behaviors (proliferation, differentiation and death) were not biased to a particular lamina (**Supplementary Fig. 7**). On each day, 3% of NG2⁺ cells were engaged in these dynamic behaviors (**Fig. 3d**), which expanded to include 36% of the population over 2 weeks. Notably, cell loss through death or differentiation

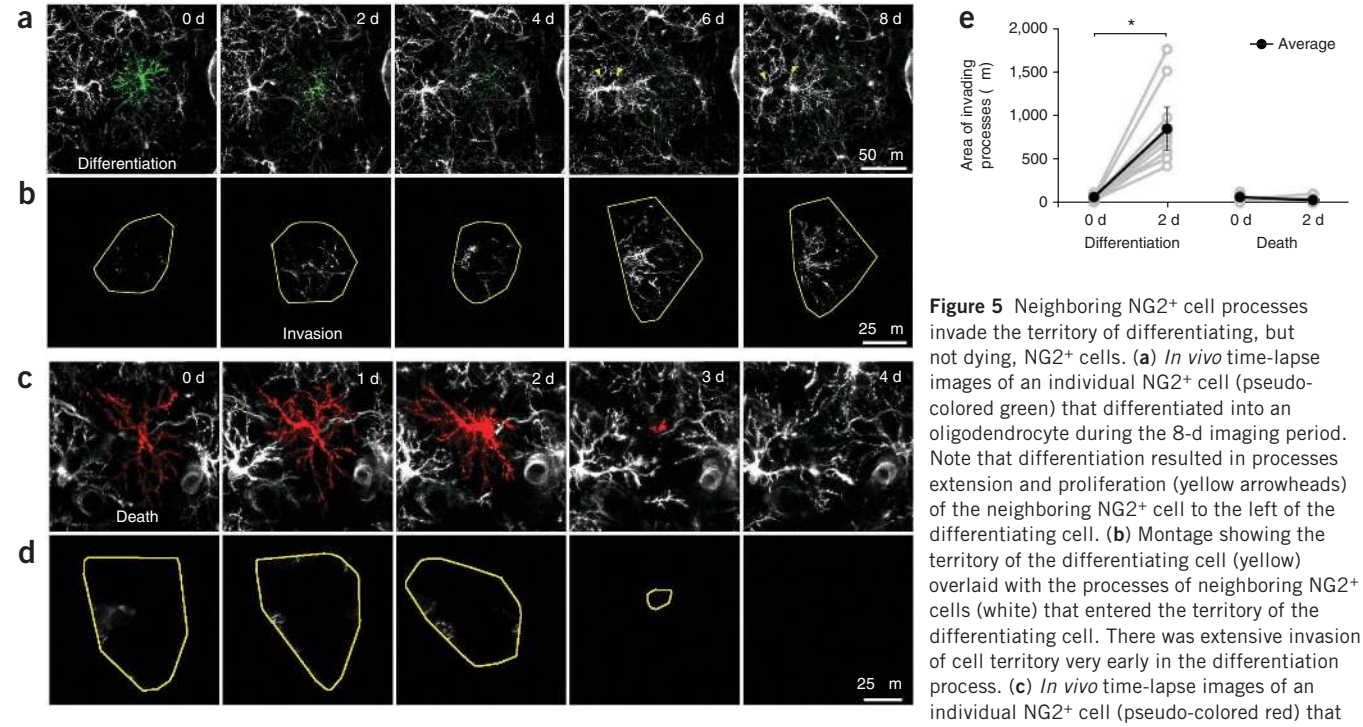

Figure 5 Neighboring NG2⁺ cell processes invade the territory of differentiating, but not dying, NG2⁺ cells. (**a**) *In vivo* time-lapse images of an individual NG2⁺ cell (pseudo-colored green) that differentiated into an oligodendrocyte during the 8-d imaging period. Note that differentiation resulted in processes extension and proliferation (yellow arrowheads) of the neighboring NG2⁺ cell to the left of the differentiating cell. (**b**) Montage showing the territory of the differentiating cell (yellow) overlaid with the processes of neighboring NG2⁺ cells (white) that entered the territory of the differentiating cell. There was extensive invasion of cell territory very early in the differentiation process. (**c**) *In vivo* time-lapse images of an individual NG2⁺ cell (pseudo-colored red) that died during the 4-d imaging period. (**d**) Montage showing the territory of the dying cell (yellow) overlaid with the processes of neighboring NG2⁺ cells (white) that entered the territory of the dying cell. Scale bar applies to both **c** and **d**. (**e**) Area of processes that invaded the territory of differentiating or dying NG2⁺ cells (10 differentiating, 10 dying NG2⁺ cells in 5 mice, $^{*}P < 0.0005$, paired two-tailed Student's *t* test). Error bars represent s.e.m.

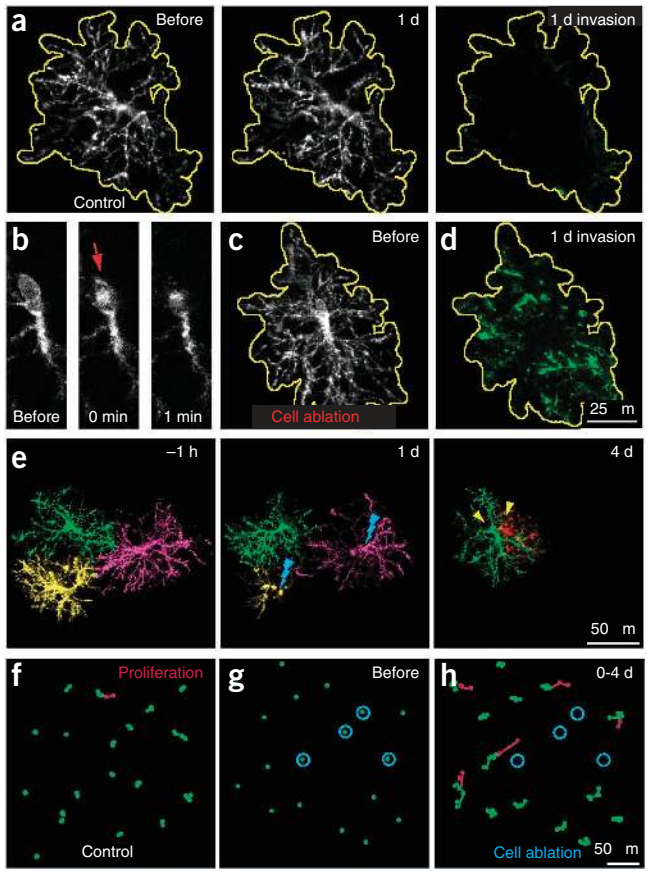

Figure 6 NG2+ cell ablation triggers territory invasion and division of a neighboring NG2+ cell. (**a**) *In vivo* time-lapse images of an individual NG2+ cell over 1 d. The territory of the cell is outlined in yellow. Processes of neighboring NG2+ cells have been pseudo-colored green. Note the lack of territory invasion over 1 d (far right, invasion). (**b**) Single *Z* plane images of an individual NG2+ cell before and after brief exposure of the cell body to the focused laser beam to induce ablation. The red arrow highlights the increase in autofluorescence of the nucleus after illumination. Panel width = 17 µm. (**c**) Maximum intensity projection image of the NG2+ cell shown in **b** before ablation. The territory of the cell is outlined in yellow. (**d**) Montage of the same volume of tissue in **c** 1 d following cell ablation. Processes of neighboring NG2+ cells have been pseudo-colored green. Scale bar applies to **a**, **c** and **d**. (**e**) *In vivo* time-lapse images of three neighboring NG2+ cells (pseudo-colored green, yellow and magenta) from a thinned-skull preparation. Two NG2+ cells (shown in yellow and magenta) were removed by laser-mediated ablation on day 1. On day 4, a neighboring NG2+ cell (green) divided (yellow arrowheads). (**f**) Map of the soma position of NG2+ cells over 4 d in control. Newly generated NG2+ cells are represented in red. (**g**) Snapshot of NG2+ cells distribution before cell ablation. Cells to be targeted for ablation are circled in blue. (**h**) Map of the soma position of NG2+ cells over 4 d following ablation of four NG2+ cells (shown in **g**). Newly generated NG2+ cells are represented in red.

$(1.2 \pm 0.1\%\ d^{-1})$ was balanced by cell addition through proliferation $(1.5 \pm 0.1\%\ d^{-1}$, $P = 0.09)$, allowing the density of NG2+ cells to remain constant (0 d, 162 NG2+ cells; 14 d, 159 NG2+ cells; 5 mice, $P = 0.9$, unpaired two-tailed Student's *t* test; **Fig. 3e**), indicating that this progenitor pool is constantly reorganized by the continual loss and addition of new cells.

NG2+ cell density is maintained through local proliferation

If homeostatic control of NG2+ cell density is governed by local interactions, then differentiation or death should be associated with division of a neighboring cell. We observed that 98% of differentiating and 76% of dying NG2+ cells were associated with the proliferation of a neighboring NG2+ cell (<50 µm away), whereas only 43% of stable NG2+ cells were associated with a local proliferation ($P < 0.005$ for both death and differentiation; **Fig. 4a–c**). Moreover, the probability of local proliferation in instances of death or differentiation was highest at the time of cell loss, but did not vary with time for control NG2+ cells (**Fig. 4d**). Neighboring NG2+ cells rapidly invaded the territory of differentiating cells (**Fig. 5a**,**b**,**e**), suggesting that the homotypic repulsive cues that prevent overgrowth are downregulated with differentiation. In contrast, dying NG2+ cells maintained distinct, albeit progressively smaller, territories until removal (**Fig. 5c–e**). The gradual decrease in the territory of dying cells (**Supplementary Fig. 5**) occasionally resulted in repositioning of neighboring NG2+ cells without cell proliferation, accounting for the somewhat lower incidence of neighbor proliferation in cases of death.

To further assess whether cell loss is sufficient to induce local proliferation, we ablated individual NG2+ cells *in vivo* using focal laser illumination and examined the response of neighboring NG2+ cells. Following cell removal, neighboring NG2+ cells reoriented their processes and invaded the former territory of the ablated cell, providing

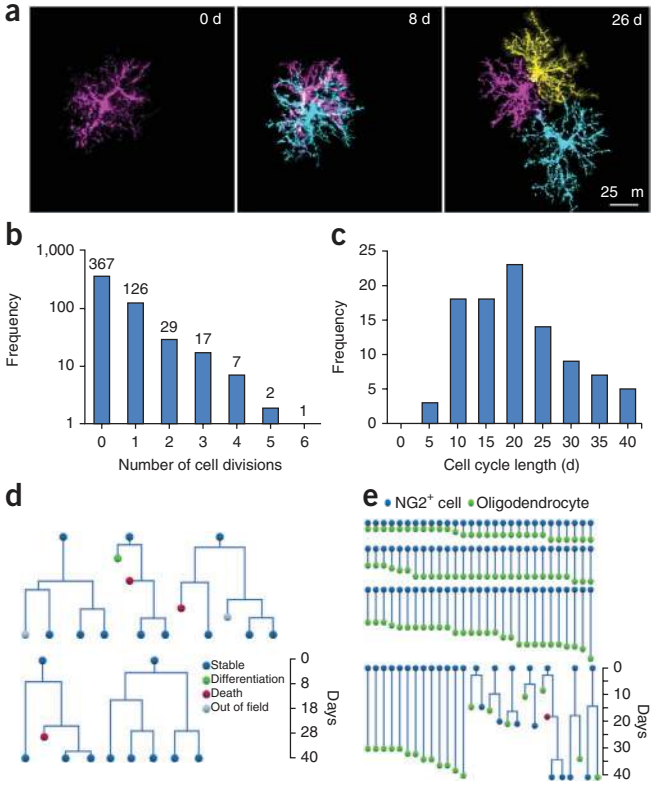

Figure 7 NG2+ cells directly differentiate into oligodendrocytes without asymmetric division. (**a**) Sequential images from *in vivo* time-lapse recordings of one NG2+ cell that divided twice over 26 d. Newly generated cells are shown in cyan and yellow. (**b**) Histogram of the distribution of proliferation frequencies of NG2+ cells in the somatosensory cortex (828 NG2+ cells in three mice imaged for 40 d). (**c**) Histogram of NG2+ cell cycle length (97 NG2+ cell divisions in 3 mice). (**d**) Lineage trees of highly proliferative NG2+ cells illustrating the range of fates of sister cells. (**e**) Lineage trees of NG2+ cells that differentiated into oligodendrocytes (107 NG2+ cells in 5 mice).

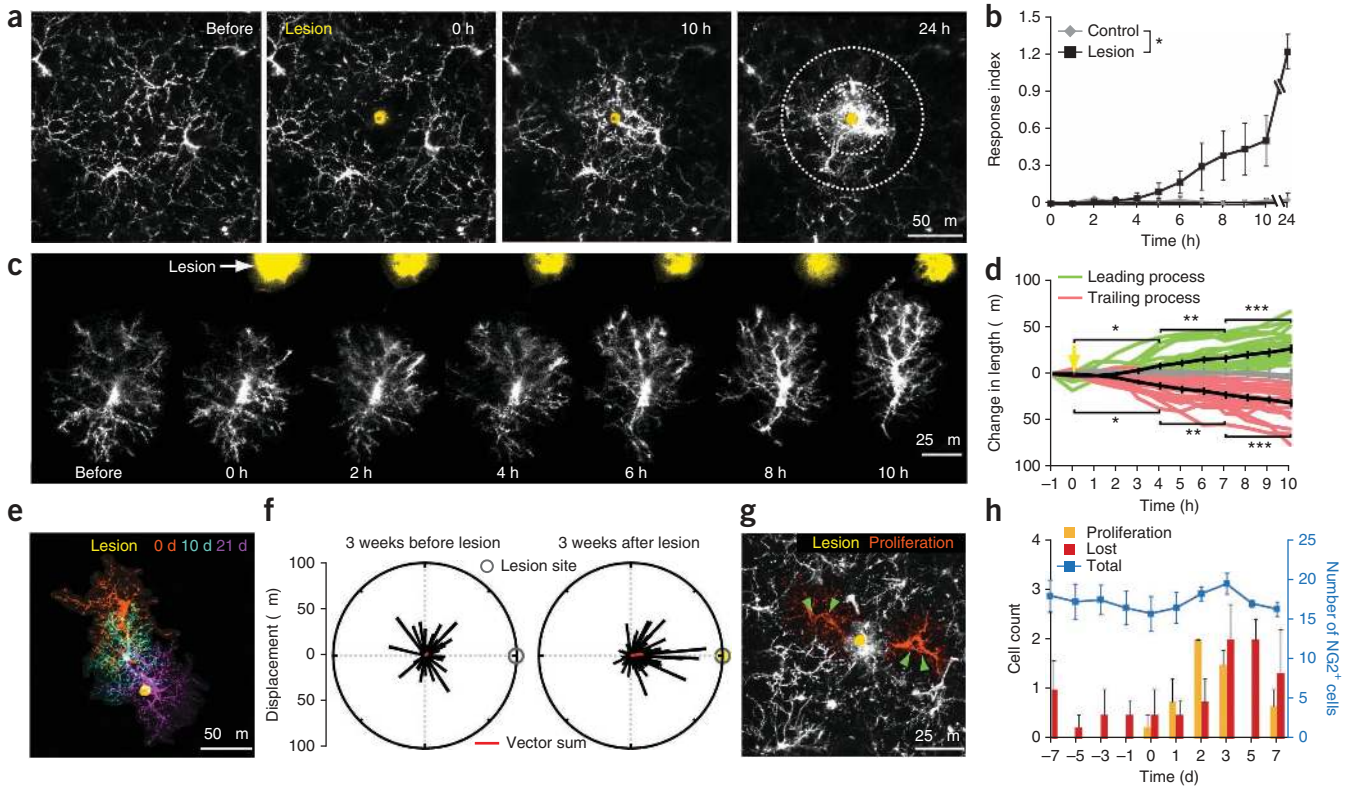

Figure 8 NG2$^+$ cells surround areas of CNS damage and proliferate to maintain their density. (**a**) Time-lapse imaging of NG2$^+$ cell responses to focal laser injury (site of lesion shown in yellow). (**b**) Graph showing accumulation of EGFP$^+$ NG2$^+$ cell processes within 75 µm of the lesion over time. Concentric circles on the 24-h time point in **a** highlight the areas measured to determine the response index ($n = 5$ mice per condition, $^*P < 0.05$, two-way ANOVA). (**c**) Sequential images showing the response of a NG2$^+$ cell to a focal laser injury (yellow spot). (**d**) Quantification of extension and retraction of leading and trailing processes of NG2$^+$ cells relative to the lesion ($n = 20$ branches on 10 cells in 4 mice; $^*P < 0.05$, $^{**}P < 0.005$, $^{***}P < 0.0005$, one-way ANOVA with Tukey *post hoc* test). (**e**) Montage of three images of one NG2$^+$ cell collected on different days showing the migration of the cell toward the lesion (yellow). (**f**) Vector plots showing the direction and displacement of NG2$^+$ cells within 75 µm of the lesion site 3 weeks before and after lesion induction (73 cells in 4 mice; before, $P = 0.073$; after, $P = 1.02 \times 10^{-9}$, Moore-Rayleigh test). Line direction represents the angle of the displacement relative to the lesion site. Red line is the vector sum of all displacements. (**g**) Maximum-intensity projection of 15 µm above and below a focal laser injury (yellow) 2 d after lesion induction. Two proliferating NG2$^+$ cells (green arrowheads) adjacent to the lesion site are highlighted in orange. (**h**) Combined plot showing the number of NG2$^+$ cells undergoing proliferation and death and/or differentiation (combined) and the total NG2$^+$ cell density (blue line) within 75 µm of the lesion. Focal laser injury was induced on day 0 ($n = 4$ mice). Error bars represent s.e.m.

further evidence that NG2$^+$ cell domains are maintained by self-avoidance (percent territory invasion: control, 6 ± 1%, $n = 10$ cells; cell ablation, 52 ± 10%, $n = 12$ cells; $P < 0.001$, Student's t test; **Fig. 6a–d**). Moreover, removal of several NG2$^+$ cells in the imaging field triggered reorientation, cell migration and proliferation of NG2$^+$ cells in the vicinity, resulting in the rapid restoration of their density (number of proliferating cells: control, 1 ± 0.4 cells; cell ablation, 5 ± 0.3 cells; volume analyzed = 0.02 mm^3, from four control and three ablation mice; $^*P < 0.001$, Student's t test; **Fig. 6e–h**). These data indicate that NG2$^+$ cells maintain a constant density using a local homeostatic mechanism in which cell loss results in release from growth inhibition and rapid replacement through division of a neighboring cell.

NG2$^+$ cells directly differentiate into oligodendrocytes

NG2$^+$ cells in the adult CNS can be generated from SVZ progenitors[32], which may have a greater capacity for proliferation and differentiation than cells with a longer residence time. To determine whether repopulation is accomplished by a subset of highly proliferative, self-renewing NG2$^+$ cells[33], we followed the behavior of proliferating NG2$^+$ cells by repeatedly imaging the same cortical volume for many weeks. During this period, the majority of proliferating NG2$^+$ cells divided only once, and, for cells that divided multiple times, cell cycle length was variable (average cell cycle, 18.5 ± 1 d, $n = 97$ cells; **Fig. 7a–c**), as would be expected if extrinsic factors (that is, death or differentiation of a neighbor) determine when NG2$^+$ cells divide. Indeed, cells that underwent multiple divisions were located in regions in which there was substantial turnover or differentiation. Moreover, lineage trees of highly proliferative cells revealed instances in which both sister cells underwent multiple divisions, as well as instances in which one sister cell either died or differentiated and the other remained stable (**Fig. 7d**). These findings, and the consistent proliferation of immediate neighbors following cell loss, suggest that homeostasis is achieved by endowing all NG2$^+$ cells with the capacity to divide[7], rather than by seeding the brain with a subset of highly proliferative cells.

New neurons are formed in the CNS through symmetric or asymmetric division of progenitors[34]; however, it is unclear whether oligodendrocytes are formed through similar mechanisms or by direct differentiation of NG2$^+$ cells[20]. Lineage tracing through *in vivo* imaging revealed that differentiation was rarely preceded by cell division (7 of 107 differentiation events; **Fig. 7e**), indicating that oligodendrocytes in the adult CNS are primarily formed through direct

differentiation of these progenitors. Thus, proliferation of NG2$^+$ cells *in vivo* reflects a homeostatic response to cell depletion rather than oligodendrogenesis.

NG2$^+$ cells participate in glial scar formation

NG2$^+$ cell proliferation is often enhanced after injury and the NG2 proteoglycan accumulates at lesion sites, where it can inhibit axon outgrowth[18,35]. However, the reason for the enhanced proliferation of these cells is unknown and the participation of NG2$^+$ cells in scar formation has not been established, as NG2 is also expressed by macrophages and pericytes in injured tissue[36,37]. To assess the behavior of NG2$^+$ glial cells to CNS injury, we induced focal laser lesions[25] in the cortex of adult *NG2-mEGFP-H* mice. Immediately following injury, NG2$^+$ cells adjacent to the lesion extended processes toward the lesion site and eventually surrounded the site of injury (**Fig. 8a–d** and **Supplementary Movie 7**). Although their response to focal injury was similar to microglia[25], NG2$^+$ cells extended their processes more slowly than microglia to the lesion site (**Fig. 8b**). As a consequence, scars acquired a layered structure consisting of microglial cell processes surrounded by NG2$^+$ cell processes (**Supplementary Fig. 8**).

Reorientation and extension of NG2$^+$ cell processes after injury was followed by migration of these cells to the lesion site in several weeks, and eventual removal of these cells as the scar resolved (**Fig. 8e,f** and **Supplementary Movie 8**). As predicted by their homeostatic behavior to cell loss, depletion of NG2$^+$ cells from the area surrounding the lesion was accompanied by proliferation of neighboring NG2$^+$ cells (**Fig. 8g**), with the number of proliferating cells matching the number lost (before lesion, 18 ± 2 NG2$^+$ cells; after lesion, 16 ± 1 NG2$^+$ cells; $n = 4$ mice, $P = 0.5$; **Fig. 8h**). These findings indicate that NG2$^+$ cells contribute to glial scar formation and provide an explanation for the enhanced proliferation of NG2$^+$ cells that occurs following many types of CNS trauma.

DISCUSSION

NG2$^+$ glial cells comprise the most abundant population of proliferative cells in the adult CNS. These progenitors retain the capacity to differentiate into oligodendrocytes and contribute to regeneration of myelin following injury and disease. Homeostatic control of their density and distribution allows not only efficient replacement of oligodendrocytes, but also ensures that cell growth does not proceed unchecked and result in tumor formation. To determine how NG2$^+$ cell density is maintained in the adult CNS, we developed mice that express membrane-anchored EGFP in NG2$^+$ cells (*NG2-mEGFP-H* mice) and examined the behavior of these ubiquitous progenitors in the somatosensory cortex of adult mice using *in vivo* two-photon imaging. We found that NG2$^+$ cells are highly dynamic in the resting brain; they actively surveyed their local environment with motile filopodia and continually migrated through the parenchyma, maintaining exclusive territories through self-repulsion. NG2$^+$ cells removed from the population by differentiation or death were rapidly replaced through proliferation of an immediate neighbor (**Supplementary Fig. 9**). By balancing active growth with self-repulsion, NG2$^+$ cells ensure that proliferation is coupled both spatially and temporally to cell loss, preserving a high density of these progenitors throughout the CNS to efficiently generate oligodendrocytes and participate in tissue repair.

NG2$^+$ glial cells are distributed in a grid-like or tiled manner in the adult CNS, with individual cells occupying non-overlapping domains. As this grid is constantly reorganized, mechanisms must exist to actively limit the growth of these progenitors. In the mammalian retina, the mosaic spacing of neurons is regulated by homotypic repulsive interactions through transmembrane receptors (for example, MEGFs and DSCAM)[27,38]. Similar repulsive interactions are likely to be involved in both establishing and maintaining the density of NG2$^+$ cells, as selective ablation of individual NG2$^+$ cells was sufficient to trigger rapid invasion of the territory of the removed cell, and contact between NG2$^+$ cell processes was always followed by retraction (**Figs. 1** and **6**). Homotypic repulsion would also provide the means to establish and maintain the radial orientation of their processes[28]. Alternatively, proliferation of these progenitors may be triggered by enhanced access to mitogens, such as platelet-derived growth factor (PDGF), as overexpression of PDGF increases the number of oligodendrocyte progenitors in the developing spinal cord[39] and induces tumors from these cells in adults[40]. However, oligodendrocyte progenitors exhibit a density-dependent reduction in proliferation in saturating PDGF *in vitro*[41], suggesting that direct interactions can limit their growth. Although guidance cues, such as netrin and semaphorins, have been shown to influence the dispersion and differentiation of oligodendrocyte progenitors during development[31], the molecules that maintain their density in the adult CNS remain unknown. As NG2$^+$ cell processes overlap extensively with other glial cells that exhibit tiling, such as astrocytes and microglia, the molecular pathways that control the distribution and density of different glial cell types are likely to be distinct.

Long-term time-lapse imaging of NG2$^+$ cells in the cortex revealed that the entire network of NG2$^+$ cells is constantly reorganized as a result of the continual loss of cells and their intrinsic pressure to actively survey their local environment. The migration of individual cells was induced by local events—the differentiation, death or displacement of neighboring cells—rather than large-scale attractive or repulsive gradients (**Fig. 2d**). In some instances, multiple cells in the imaged volume died or differentiated, creating larger voids that resulted in greater reorganization through migration of nearby NG2$^+$ cells. However, large-scale migration of individual cells through the parenchyma was not observed and maintenance of the population was achieved through local proliferation of neighboring cells, rather than through a subpopulation of highly migratory, proliferative NG2$^+$ cells (**Fig. 7d**), consistent with the marked self-avoidance exhibited by these cells.

Dynamic filopodia were distributed along the length of NG2$^+$ cells processes and even projected from their somata. This constant exploration of the local environment by NG2$^+$ cells may allow them to not only assess their density, but also the viability of oligodendrocytes and the state of myelination of nearby axons[4]. If local interactions are required to stimulate oligodendrogenesis, it would explain why a high density of these progenitors is maintained throughout the adult CNS. In multiple sclerosis, NG2$^+$ cell density is markedly reduced in many chronically demyelinated white matter lesions[42]. This impairment of NG2$^+$ cell homeostasis may prevent detection of demyelinated axons and limit oligodendrocyte regeneration, raising the possibility that focal restoration of NG2$^+$ cell numbers in chronic lesions may be therapeutically beneficial in multiple sclerosis.

NG2$^+$ cells form functional synapses with glutamatergic neurons in all of the regions of the CNS that have been examined[43–45]. The high motility of NG2$^+$ cell processes and constant movement of these cells through the parenchyma contrast with the marked stability of glutamatergic axons in the cortex observed through similar *in vivo* imaging, which, apart from the refinement of some boutons, do not change their position over several months[46]. The extent of NG2$^+$ cell movement suggests that synaptic connections between axons and NG2$^+$ cells are continually remodeled on a time scale of days to weeks.

The transient nature of these synapses may explain why NG2$^+$ cells in the same brain region exhibit widely varying levels of synaptic connectivity[45]. Although the role of this rapid form of neuron-glial cell communication has not been established *in vivo*, glutamatergic signaling influences the proliferation and differentiation of these progenitors *in vitro*[47]. As NG2$^+$ cells occupy non-overlapping domains, the continual reorganization of their processes may enable these progenitors to sample the activity of a greater proportion of axons to enable learning-induced changes in myelination[48], and ensure that oligodendrocytes that degenerate as a result of injury, disease or normal aging are rapidly replaced.

In vivo genetic fate tracing studies have suggested that NG2$^+$ cells continue to generate oligodendrocytes in the adult CNS, although less frequently than during early postnatal life[7,11–13]. Consistent with these findings, our time-lapse imaging revealed that NG2$^+$ cells in the cortex of 5-month-old mice continued to differentiate into oligodendrocytes at a low rate (**Fig. 3**). *In vitro* studies indicate that oligodendrocytes are generated through asymmetric division of these progenitors[20]; however, the steps leading to oligodendrogenesis *in vivo* remain uncertain. Using long-term imaging, we discovered that the majority of NG2$^+$ cells in the adult cortex directly differentiated into oligodendrocytes without undergoing asymmetric division. Thus, proliferation of NG2$^+$ cells *in vivo* is not a direct reflection of oligodendrogenesis, but rather a homeostatic response to replace progenitors that have differentiated or died.

Our analysis of NG2$^+$ cells focused exclusively on layers 1 and 2/3 of the cortex as a result of the limitations of two-photon imaging at greater depths. Although each cortical layer has a distinct cytoarchitecture, NG2$^+$ cell behavior was similar throughout these upper layers of cortex (**Supplementary Fig. 7**), consistent with the ability of these cells to proliferate and generate new oligodendrocytes throughout the CNS[7,13]. Although not considered a traditional white matter region, layer 1 of the cortex contains a relatively high density of myelinated axons that course horizontally through the dendritic tufts of pyramidal neurons. Nevertheless, it is possible that NG2$^+$ cell behaviors may differ between gray and white matter in the adult CNS, particularly if these regions vary with regard to cell turnover or oligodendrogenesis. The development of new approaches for high-resolution imaging in deep brain structures such as the corpus callosum or long-term imaging of dorsal column white matter in the spinal cord will be required to examine NG2$^+$ cell behavior in adult white matter.

Injury to the CNS, whether induced acutely or through chronic disease, is often associated with gliosis, characterized by enhanced proliferation and accumulation of glia around lesions to form glial scars. This recruitment of glia to sites of trauma is thought to be crucial for limiting further injury and promoting repair. In addition to astrocytes, microglia and macrophages, cells that express the NG2 proteoglycan accumulate at lesions, with their numbers peaking 1 week after injury and then declining slowly over an extended period[37,49]. Determining the source of NG2 has been problematic, as NG2 is also expressed by pericytes and a subset of microglia and macrophages following injury[36,37] and can be released into the extracellular space through enzymatic cleavage by matrix metalloproteinases[50]. Time-lapse imaging of individual NG2$^+$ cells revealed that these progenitors are attracted to the site of injury in a manner similar to microglia[25]; they reorient and extend their processes toward the lesion and eventually migrate to the peri-lesion area to participate in the formation of the scar. NG2$^+$ cells recruited to the lesion no longer exhibit self-repulsion, suggesting that injury may transform these cells into distinct scar-forming cells with unique characteristics. Accordingly, loss of cells to the scar triggered homeostatic proliferation of surrounding NG2$^+$ cells to restore their density. Although NG2$^+$ cells began to reorient their processes within minutes of injury, they arrived at the lesion several hours later than microglia (extension rate: NG2$^+$ cells, $2.7 \pm 0.4\ \mu m\ h^{-1}$, **Fig. 8**; microglia, $1.25 \pm 0.06\ \mu m\ min^{-1}$, from ref. 25). The sequential appearance of these different types of glial cells at the lesion suggests that they have distinct roles in the response to acute injury. Long-term time-lapse imaging revealed that accumulation of NG2$^+$ cell processes reached its peak 1 week following injury induction (**Supplementary Movie 8**) and were eventually removed as the scar resolved. The participation of NG2$^+$ cells in the formation and resolution of glial scars suggests that that these ubiquitous progenitors not only serve as a reservoir to generate oligodendrocytes, but also as a surveillance network to detect CNS injury and promote tissue repair.

METHODS

Methods and any associated references are available in the online version of the paper.

Note: Supplementary information is available in the online version of the paper.

ACKNOWLEDGMENTS

We thank M. Pucak, N. Ye and T. Lee for technical assistance, B. Cudmore (Johns Hopkins University) and S. Wang (Princeton University) for advice on cranial window implantation, W.-B. Gan (New York University) for advice on preparing thinned skull windows, and members of the Bergles laboratory for discussions. E.G.H. was supported by a Kirschstein National Research Service Award grant from the US National Institutes of Health (F32NS076098). Funding was provided by grants from the US National Institutes of Health (NS051509, NS050274) and the Brain Science Institute at Johns Hopkins University.

AUTHOR CONTRIBUTIONS

E.G.H., M.F., S.H.K. and D.E.B. designed the experiments. E.G.H. designed, executed and analyzed the experiments described in the figures, movies and text. M.F. made seminal observations of NG2$^+$ cell dynamics and their response to laser-induced lesions in thinned skull preparations, and generated data for **Supplementary Figure 8**. S.H.K. generated and characterized the *NG2-mEGFP-H* and *NG2-mEGFP-L* mouse lines and created **Supplementary Figure 1**. E.G.H. and D.E.B. wrote the manuscript.

COMPETING FINANCIAL INTERESTS

The authors declare no competing financial interests.

1. Biteau, B., Hochmuth, C.E. & Jasper, H. Maintaining tissue homeostasis: dynamic control of somatic stem cell activity. *Cell Stem Cell* **9**, 402–411 (2011).
2. Simons, B.D. & Clevers, H. Strategies for homeostatic stem cell self-renewal in adult tissues. *Cell* **145**, 851–862 (2011).
3. Zhao, C., Deng, W. & Gage, F.H. Mechanisms and functional implications of adult neurogenesis. *Cell* **132**, 645–660 (2008).
4. Franklin, R.J., Gilson, J.M. & Blakemore, W.F. Local recruitment of remyelinating cells in the repair of demyelination in the central nervous system. *J. Neurosci. Res.* **50**, 337–344 (1997).
5. Ajami, B., Bennett, J.L., Krieger, C., Tetzlaff, W. & Rossi, F.M. Local self-renewal can sustain CNS microglia maintenance and function throughout adult life. *Nat. Neurosci.* **10**, 1538–1543 (2007).
6. Dawson, M.R., Polito, A., Levine, J.M. & Reynolds, R. NG2-expressing glial progenitor cells: an abundant and widespread population of cycling cells in the adult rat CNS. *Mol. Cell Neurosci.* **24**, 476–488 (2003).
7. Kang, S.H., Fukaya, M., Yang, J.K., Rothstein, J.D. & Bergles, D.E. NG2$^+$ CNS glial progenitors remain committed to the oligodendrocyte lineage in postnatal life and following neurodegeneration. *Neuron* **68**, 668–681 (2010).
8. Kessaris, N. *et al.* Competing waves of oligodendrocytes in the forebrain and postnatal elimination of an embryonic lineage. *Nat. Neurosci.* **9**, 173–179 (2006).
9. Kirby, B.B. *et al. In vivo* time-lapse imaging shows dynamic oligodendrocyte progenitor behavior during zebrafish development. *Nat. Neurosci.* **9**, 1506–1511 (2006).

10. Nishiyama, A., Komitova, M., Suzuki, R. & Zhu, X. Polydendrocytes (NG2 cells): multifunctional cells with lineage plasticity. *Nat. Rev. Neurosci.* **10**, 9–22 (2009).
11. Rivers, L.E. *et al.* PDGFRA/NG2 glia generate myelinating oligodendrocytes and piriform projection neurons in adult mice. *Nat. Neurosci.* **11**, 1392–1401 (2008).
12. Dimou, L., Simon, C., Kirchhoff, F., Takebayashi, H. & Gotz, M. Progeny of Olig2-expressing progenitors in the gray and white matter of the adult mouse cerebral cortex. *J. Neurosci.* **28**, 10434–10442 (2008).
13. Young, K.M. *et al.* Oligodendrocyte dynamics in the healthy adult CNS: evidence for myelin remodeling. *Neuron* **77**, 873–885 (2013).
14. Tripathi, R.B., Rivers, L.E., Young, K.M., Jamen, F. & Richardson, W.D. NG2 glia generate new oligodendrocytes, but few astrocytes, in a murine experimental autoimmune encephalomyelitis model of demyelinating disease. *J. Neurosci.* **30**, 16383–16390 (2010).
15. Levine, J.M. & Reynolds, R. Activation and proliferation of endogenous oligodendrocyte precursor cells during ethidium bromide-induced demyelination. *Exp. Neurol.* **160**, 333–347 (1999).
16. Haber, M., Vautrin, S., Fry, E.J. & Murai, K.K. Subtype-specific oligodendrocyte dynamics in organotypic culture. *Glia* **57**, 1000–1013 (2009).
17. Haberlandt, C. *et al.* Gray matter NG2 cells display multiple Ca^{2+}-signaling pathways and highly motile processes. *PLoS ONE* **6**, e17575 (2011).
18. McTigue, D.M., Wei, P. & Stokes, B.T. Proliferation of NG2-positive cells and altered oligodendrocyte numbers in the contused rat spinal cord. *J. Neurosci.* **21**, 3392–3400 (2001).
19. Magnus, T. *et al.* Adult glial precursor proliferation in mutant SOD1G93A mice. *Glia* **56**, 200–208 (2008).
20. Sugiarto, S. *et al.* Asymmetry-defective oligodendrocyte progenitors are glioma precursors. *Cancer Cell* **20**, 328–340 (2011).
21. Ivkovic, S., Canoll, P. & Goldman, J.E. Constitutive EGFR signaling in oligodendrocyte progenitors leads to diffuse hyperplasia in postnatal white matter. *J. Neurosci.* **28**, 914–922 (2008).
22. Liu, C. *et al.* Mosaic analysis with double markers reveals tumor cell of origin in glioma. *Cell* **146**, 209–221 (2011).
23. Persson, A.I. *et al.* Non-stem cell origin for oligodendroglioma. *Cancer Cell* **18**, 669–682 (2010).
24. Benediktsson, A.M., Schachtele, S.J., Green, S.H. & Dailey, M.E. Ballistic labeling and dynamic imaging of astrocytes in organotypic hippocampal slice cultures. *J. Neurosci. Methods* **141**, 41–53 (2005).
25. Davalos, D. *et al.* ATP mediates rapid microglial response to local brain injury *in vivo*. *Nat. Neurosci.* **8**, 752–758 (2005).
26. Nimmerjahn, A., Kirchhoff, F. & Helmchen, F. Resting microglial cells are highly dynamic surveillants of brain parenchyma *in vivo*. *Science* **308**, 1314–1318 (2005).
27. Kay, J.N., Chu, M.W. & Sanes, J.R. MEGF10 and MEGF11 mediate homotypic interactions required for mosaic spacing of retinal neurons. *Nature* **483**, 465–469 (2012).
28. Lefebvre, J.L., Kostadinov, D., Chen, W.V., Maniatis, T. & Sanes, J.R. Protocadherins mediate dendritic self-avoidance in the mammalian nervous system. *Nature* **488**, 517–521 (2012).
29. Xu, H.T., Pan, F., Yang, G. & Gan, W.B. Choice of cranial window type for *in vivo* imaging affects dendritic spine turnover in the cortex. *Nat. Neurosci.* **10**, 549–551 (2007).
30. Yang, G., Pan, F., Parkhurst, C.N., Grutzendler, J. & Gan, W.B. Thinned-skull cranial window technique for long-term imaging of the cortex in live mice. *Nat. Protoc.* **5**, 201–208 (2010).
31. Spassky, N. *et al.* Directional guidance of oligodendroglial migration by class 3 semaphorins and netrin-1. *J. Neurosci.* **22**, 5992–6004 (2002).
32. Menn, B. *et al.* Origin of oligodendrocytes in the subventricular zone of the adult brain. *J. Neurosci.* **26**, 7907–7918 (2006).
33. Psachoulia, K., Jamen, F., Young, K.M. & Richardson, W.D. Cell cycle dynamics of NG2 cells in the postnatal and ageing brain. *Neuron Glia Biol.* **5**, 57–67 (2009).
34. Kriegstein, A. & Alvarez-Buylla, A. The glial nature of embryonic and adult neural stem cells. *Annu. Rev. Neurosci.* **32**, 149–184 (2009).
35. Busch, S.A. & Silver, J. The role of extracellular matrix in CNS regeneration. *Curr. Opin. Neurobiol.* **17**, 120–127 (2007).
36. Göritz, C. *et al.* A pericyte origin of spinal cord scar tissue. *Science* **333**, 238–242 (2011).
37. Jones, L.L., Yamaguchi, Y., Stallcup, W.B. & Tuszynski, M.H. NG2 is a major chondroitin sulfate proteoglycan produced after spinal cord injury and is expressed by macrophages and oligodendrocyte progenitors. *J. Neurosci.* **22**, 2792–2803 (2002).
38. Fuerst, P.G., Koizumi, A., Masland, R.H. & Burgess, R.W. Neurite arborization and mosaic spacing in the mouse retina require DSCAM. *Nature* **451**, 470–474 (2008).
39. Calver, A.R. *et al.* Oligodendrocyte population dynamics and the role of PDGF *in vivo*. *Neuron* **20**, 869–882 (1998).
40. Assanah, M.C. *et al.* PDGF stimulates the massive expansion of glial progenitors in the neonatal forebrain. *Glia* **57**, 1835–1847 (2009).
41. Zhang, H. & Miller, R.H. Density-dependent feedback inhibition of oligodendrocyte precursor expansion. *J. Neurosci.* **16**, 6886–6895 (1996).
42. Chang, A., Nishiyama, A., Peterson, J., Prineas, J. & Trapp, B.D. NG2-positive oligodendrocyte progenitor cells in adult human brain and multiple sclerosis lesions. *J. Neurosci.* **20**, 6404–6412 (2000).
43. Chittajallu, R., Aguirre, A. & Gallo, V. NG2-positive cells in the mouse white and grey matter display distinct physiological properties. *J. Physiol. (Lond.)* **561**, 109–122 (2004).
44. Bergles, D.E., Roberts, J.D., Somogyi, P. & Jahr, C.E. Glutamatergic synapses on oligodendrocyte precursor cells in the hippocampus. *Nature* **405**, 187–191 (2000).
45. De Biase, L.M., Nishiyama, A. & Bergles, D.E. Excitability and synaptic communication within the oligodendrocyte lineage. *J. Neurosci.* **30**, 3600–3611 (2010).
46. De Paola, V. *et al.* Cell type–specific structural plasticity of axonal branches and boutons in the adult neocortex. *Neuron* **49**, 861–875 (2006).
47. Gallo, V. *et al.* Oligodendrocyte progenitor cell proliferation and lineage progression are regulated by glutamate receptor–mediated K^+ channel block. *J. Neurosci.* **16**, 2659–2670 (1996).
48. Bengtsson, S.L. *et al.* Extensive piano practicing has regionally specific effects on white matter development. *Nat. Neurosci.* **8**, 1148–1150 (2005).
49. Levine, J.M. Increased expression of the NG2 chondroitin-sulfate proteoglycan after brain injury. *J. Neurosci.* **14**, 4716–4730 (1994).
50. Larsen, P.H., Wells, J.E., Stallcup, W.B., Opdenakker, G. & Yong, V.W. Matrix metalloproteinase-9 facilitates remyelination in part by processing the inhibitory NG2 proteoglycan. *J. Neurosci.* **23**, 11127–11135 (2003).

ONLINE METHODS

Generation of *NG2-mEGFP* transgenic mice. A mouse bacterial artificial chromosome (BAC) clone containing the *NG2* (*Cspg4*) gene (RP23-309G21) was purchased from BACPAC Resources Center and modified by homologous recombination[51]. To target EGFP to the plasma membrane, the first 26 amino acids of Lck, a Src family tyrosine kinase that contains two palmitoylation domains and a myristoylation domain (gift from M. Dailey and S. Green, University of Iowa)[24], was fused to the N terminus of EGFP in pEGFP-N1 (Clontech). A cDNA encoding this membrane-anchored EGFP (mEGFP) and subsequent rabbit β-globin polyA signal were placed at the translational initiator (ATG) of the *NG2* (*Cspg4*) gene with two flanking homology arms (500 bp for each arm). The modified BAC was linearized by NotI digestion, injected into the pronucleus of mouse embryos in the John Hopkins University Transgenic Core and implanted into pseudopregnant females. Of the three lines of *NG2-mEGFP* mice generated, two lines were selected for further studies.

***In vivo* two-photon microscopy.** All experiments were performed in strict accordance with protocols approved by the Animal Care and Use Committee at Johns Hopkins University. To prepare cranial windows, *NG2-mEGFP-H* mice (2–3 months old) were anesthetized by interperitoneal injection of ketamine (100 mg per kg of body weight) and xylazine (10 mg per kg); body temperature was maintained at 37 °C with a thermostat-controlled heating plate. The skin over the right cerebral hemisphere was retracted and the skull cleaned. A metal plate with a center hole was attached to the skull with dental cement (C&B Metabond) to allow for head stabilization. A ~400-μm-diameter region of skull over somatosensory cortex (−0.5 to −2 mm post bregma and 1 to 3.5 mm lateral) was either thinned (~20 μm thickness) or removed using a high-speed dental drill[30,52]. For cranial windows, a piece of cover glass (VWR, No. 1) was placed in the craniotomy and sealed with dental cement. *In vivo* imaging sessions began immediately after surgery (thinned-skull preparation) or after a minimum of 3 weeks (chronic cranial window). Although craniotomy can induce gliosis[29], these small cranial windows did not induce reactive changes in microglial cells or NG2$^+$ cells 3 weeks following implantation (**Supplementary Fig. 4**). Mice were anesthetized with isoflurane (1.0–1.5%, mixed with 0.5 l min^{-1} O_2) during imaging. Images were collected using a Zeiss LSM 710 microscope equipped with a GaAsP detector using a mode-locked Ti:sapphire laser (Coherent Ultra II) tuned to 920 nm. The average power at the sample during imaging was <30 mW. Vascular landmarks (EGFP$^+$ pericytes) were used to identify the same imaging area on subsequent days.

Two-photon laser-induced lesions and individual cell ablation. Small lesions were induced in cortical gray matter by illuminating with the Ti:sapphire laser for several seconds (780 nm, ~150 mW, 1–3 s)[25]. This protocol induced a ~20-μm area of damage visible as an autofluorescent sphere. To ablate individual NG2$^+$ cells in mice with thinned-skull windows, cell somata were subjected to repeated, short-duration laser irradiation (780 nm, ~150 mW, 100–500 ms, 1–6 repetitions)[53]. Successful ablations were preceded by slight swelling of the soma that was followed by cell disappearance within 1–8 h. Laser power, pulse duration and pulse repetition were varied depending on the depth of the targeted cell and thickness of the overlying thinned-skull.

Image processing and analysis. Image stacks and times series were analyzed using Fiji[54]. All analysis was performed on unprocessed images. For presentation in figures, image brightness and contrast levels were adjusted for clarity. Filopodial images were additionally processed with a Gaussian filter (radius = 2 pixels) to remove detector noise. For pseudo-color display of individual cells, the three-dimensional cell volume was defined plane-by-plane for each time point and a custom Fiji script was used to segment and/or colorize the cell.

Filopodial analysis. Filopodia on NG2$^+$ cell processes (≥50 μm in length) were analyzed frame by frame using a custom Fiji script to quantify filopodial length, motility, density and lifetime. Filopodia were considered to be dynamic if the length varied more than 2 μm during the imaging period. For analysis of filopodial density in fixed tissue, protrusions with a length at least twice the width and a minimum length of 2 μm were classified as filopodia.

Cell tracking. NG2$^+$ cells were tracked in three dimensions using custom Fiji scripts by defining soma position at each time point, recording *xyz* coordinates and categorizing 'cellular behavior' (for example, proliferation, differentiation, etc.). NG2$^+$ cells were classified as proliferating if two cells appeared in the same location where there was one cell at the previous time point, the somata were separated by less than 50 μm, the processes of recently divided cells were oriented in opposing directions and the somata lacked major cell processes at the point closest to the sister cell. The three-dimensional volume around each proliferating cell was examined to exclude neighboring NG2$^+$ cells that migrated into the field. NG2$^+$ cells were classified as differentiating if the cells exhibited a progressive decrease in EGFP fluorescence, the cells changed from having radial, highly branched processes to having long, unbranched processes characteristic of oligodendrocytes, and the processes of neighboring NG2$^+$ cells invaded the territory of the differentiating cell. NG2$^+$ cells were classified as dying if cells exhibited a shortening and/or blebbing of processes, a reduction in territory size, an increase in brightness of the cell soma and a complete disappearance of EGFP fluorescence in <3 d without movement from the imaging area. NG2$^+$ cells that lost EGFP fluorescence, but could not be definitively identified as differentiated or dying, were classified as 'unsure.'

NG2$^+$ cell territory invasion. To calculate territory invasion following death or differentiation, we computed a convex hull plane by plane for each time point around the differentiating and/or dying cell, the cell masked and EGFP$^+$ processes contained in the convex hull autothresholded using the Fiji IsoData algorithm. A maximum projection of three-dimensional volume defined by the convex hull was generated and the area of processes for each time point determined. To calculate territory invasion following NG2$^+$ cell ablation, the three-dimensional volume of the ablated cell was merged with the image of the following time point to identify invading processes. For control cells, the cell in the second time point was masked and the region of the three-dimensional volume of the cell in the first time point was overlaid onto the second time point. A maximum projection of three-dimensional volume of the invading processes was autothresholded using the Fiji IsoData algorithm and the extent of territory invasion calculated by normalizing the area occupied by invading processes at the last time point to the area occupied by the cell at the first time point.

Analysis of local proliferation. NG2$^+$ cells that underwent proliferation, differentiation or death were identified during the imaging period. For each differentiating cell, the time point at which the cell displayed a premyelinating oligodendrocyte morphology[55], and neighboring cells had begun invading that cell's territory, was marked as day 0. For each cell that died, the time point that the cell displayed altered morphology (increased brightness of cell soma and reduced territory size), immediately preceding disappearance, was marked as day 0. After identification of a NG2$^+$ cell that underwent differentiation/death, immediately adjacent NG2$^+$ cells were examined for cell division preceding and following the event. The day of proliferation was marked as the time point at which the two sister cells had undergone cytokinesis and had no adjoining processes. Cells were excluded from analysis if the entire differentiation/death process did not occur during the imaging period or if not all adjacent cells were located within the field of view. For controls, we analyzed cells that did not undergo proliferation, differentiation or cell death for the entire imaging period and did not have more than one cell division within 100 μm.

Analysis of the response to focal injury. To follow appearance of NG2$^+$ cells at lesions, EGFP$^+$ processes entering a 75-μm zone surrounding lesion sites (area X) from a larger 150-μm zone (area Y) were measured as a function of time (**Fig. 4a**)[25]. To calculate the area surrounding the lesion occupied by NG2$^+$ cell processes, images were autothresholded using the Fiji IsoData algorithm and the number of pixels was assessed. The change in pixel number over time ($R_x(t)$) compared to the initial value of pixels ($R_x(0)$) represented NG2$^+$ cell processes accumulation. To control for variations in the number NG2$^+$ cells surrounding the lesion site in different experiments, accumulation of NG2$^+$ cell processes was calculated relative to the number of processes in the outer area Y immediately following induction of the lesion ($R_y(0)$). The NG2$^+$ cell response index at any time point, ($R(t)$), is given by the equation

$$R(t) = \frac{R_x(t) - R_x(0)}{R_y(0)} \quad (1)$$

To quantify response speed, we measured the length of NG2$^+$ cell processes within 150 µm of the lesion site over time. To determine the leading and trailing processes of NG2$^+$ cells, the coordinate system was rotated so that the *y* axis passed through the lesion site at the top and the soma of the cell was located at the origin (lesion site = 90° from the cell of interest). The angle at which processes extended from the soma determined whether they were on the leading edge (0–180°) or trailing edge (181–360°) of the NG2$^+$ cell.

To determine the magnitude and direction of NG2$^+$ cell movements with respect to the lesion site, the coordinate system was rotated such that the *x* axis passed through the lesion site at the right and the start point of the cell was located at the origin (lesion site = 0° from the start point). Next, the angle θ between the displacement vector of NG2$^+$ cell movement and the *x* axis (displacement vector between the start point and the lesion site) was determined using

$$\theta_i = \arccos\left(\frac{a_i \cdot a_L}{|a_i||a_L|}\right) \quad (2)$$

where a_i is the displacement vector for the cell, i and a_L are the displacement vectors between the start point of the cell and the lesion site, respectively, $a_i \cdot a_L$ is the dot product between the two vectors, and $|a| = \sqrt{a \cdot a}$. The sign of the angle was determined by calculating the determinant of the two vectors using

$$\begin{vmatrix} a_x & a_y & a_z \\ b_x & b_y & b_z \\ c_x & c_y & c_z \end{vmatrix} = a_x b_y c_z + a_y b_z c_x + a_z b_x c_y - a_z b_y c_x - a_x b_z c_y - a_y b_x c_z \quad (3)$$

where the Cartesian coordinates of the lesion site, the start position and the final position of the NG2$^+$ cell of interest are defined as *a*, *b* and *c*, respectively.

Immunohistochemistry. Mice were administered an overdose of anesthesia (pentobarbital, 100 mg per kg, intraperitoneal), perfused transcardially with 4% formaldehyde (vol/vol, in 0.1 M phosphate buffer, pH 7.4), and their brains were extracted and postfixed in 4% formaldehyde for 4 h or overnight at 4 °C, then cryoprotected in a 30% sucrose solution (wt/vol, in phosphate-buffered saline, pH 7.4) at 4 °C for up to 36 h. Brains were frozen in TissueTek, sectioned (coronal, bregma 0.2 to −1.9 mm) at 30–50 µm thick and incubated free-floating for 1–2 h at 20–30 °C in a blocking solution (5% normal donkey serum (vol/vol), 0.3% Triton X-100 (vol/vol) in phosphate-buffered saline, pH 7.4). Sections were incubated with primary antibodies (**Supplementary Table 1**) suspended in blocking solution overnight at 4 °C on an orbital shaker. For Olig2 immunostaining, brain sections were incubated in LAB solution (Polysciences) for 10 min before blocking. For BrdU immunostaining, sections were treated with 2 N HCl at 37 °C for 30 min, and then neutralized with 0.1 M sodium borate buffer (pH 8.5) before incubation with primary antibodies. After washing in blocking solution, sections were incubated with fluorescently conjugated secondary antibodies (**Supplementary Table 2**) for 2 h at 20–30 °C and then mounted on slides with Aqua Poly/Mount (Polysciences). Images were acquired using either an epifluorescence microscope (Zeiss Axio-imager M1) and Axiovision software (Zeiss) or a confocal laser-scanning microscope (Zeiss LSM 510 Meta). For cell proliferation analysis, mice were provided with BrdU-containing drinking water (1 mg ml^{-1} supplemented with 1% sucrose) and received two injections of BrdU (50 mg per kg, intraperitoneal) per day, at least 8 h apart, for 1 week before perfusion. To analyze the effects of cranial window implantation, burr holes were drilled <1 mm outside the craniotomy area and 1 µl of dextran-conjugated rhodamine was injected into the brain to label the position of the cranial window just before the mouse was killed.

Statistical analysis. Statistical analyses were performed in OriginPro (OriginLab), Excel (Microsoft) or Fiji. Sample sizes were chosen according to the standard practice in the field. Normality of the data was tested with the Shapiro-Wilk test. Significance was determined using the Mann-Whitney test, unpaired or paired two-tailed Student's *t* test, or one-way ANOVA with Tukey *post hoc* test, as noted. All direction statistics were performed using a modification to the Rayleigh's test[56], implemented in Chemotaxis and Migration Tool (ImageJ plug-in, Ibidi).

51. Yang, X.W., Model, P. & Heintz, N. Homologous recombination based modification in *Escherichia coli* and germline transmission in transgenic mice of a bacterial artificial chromosome. *Nat. Biotechnol.* **15**, 859–865 (1997).
52. Holtmaat, A. *et al.* Long-term, high-resolution imaging in the mouse neocortex through a chronic cranial window. *Nat. Protoc.* **4**, 1128–1144 (2009).
53. Chung, S.H. & Mazur, E. Femtosecond laser ablation of neurons in *C. elegans* for behavioral studies. *Appl. Phys. A Mater. Sci. Process.* **96**, 335–341 (2009).
54. Schindelin, J. *et al.* Fiji: an open-source platform for biological-image analysis. *Nat. Methods* **9**, 676–682 (2012).
55. Trapp, B.D., Nishiyama, A., Cheng, D. & Macklin, W. Differentiation and death of premyelinating oligodendrocytes in developing rodent brain. *J. Cell Biol.* **137**, 459–468 (1997).
56. Moore, B.R. A modification of the Rayleigh test for vector data. *Biometrika* **67**, 175–180 (1980).

doi:10.1038/nn.3390